AERODYNAMIC CHARACTERISTICS OF MEMBRANE AIRFOIL COMPARED TO RIGID NACA 4412 AIRFOIL

by

CHAN MIN XHAO

Thesis submitted in fulfilment of the requirements for the Bachelor Degree of Engineering (Honours) (Aerospace Engineering)

June 2018

ENDORSEMENT

I, Chan Min Xhao hereby declare that all corrections and comments made by the supervisor and examiner have been taken consideration and rectified accordingly.

(Signature of Student)

Date:

(Signature of Supervisor)

Name:
Date:

(Signature of Examiner)

Name:
Date:

DECLARATION

This thesis is the result of my own investigation, except where otherwise stated and has not previously been accepted in substance for any degree and is not being concurrently submitted in candidature for any other degree.

(Signature of Student)

Date:

ACKNOWLEDGEMENTS

First and foremost, I would like to express my deepest gratitude for Prof. Ir. Dr. Mohd Zulkifly Abdullah, my supervisor, advisor and a teacher for his patience, guidance, wisdom, ideas, enthusiasm, encouragement and overwhelming support towards my research project. Without his assistance and advice, I could not imagine myself even completing half of what I have now. I would like to thank Dr. Noorfazreena Mohammad Kamaruddin for being willing to serve as my examiner to mark this report. I would like to add my thanks to Dr. Noorfazreena for her kindness and continuous concern for my well-being. I would like to thank Dr. Nurulasikin Mohd Suhadis for laying out a proper thesis guideline.

Next, I would like to thank Mr. Nor Ridwan bin Mohamed Yusuf making my L-beam shelving. I would like to thank Mr. Muhamad Zulkhairi Mat Saad for his skills on handling the Computer Numerical Control (CNC) milling machine to fabricate the Perspex airfoil ribs. I would like to thank Mr. Mahmud Isa for his assistance in constructing my set-up of attaching the membrane to the airfoil. I would like to thank Mr. Hasfizan Hashim for directing me on how to create the polystyrene airfoil. I would like to thank Mr. Shahril Amir bin Saleh and Mr. Mohd Suharudin B. Sulong for their guidance and accommodation of my tensile test.

Finally, I would like to thank my friends and family for their emotional support and understanding.

AERODYNAMIC CHARACTERISTICS OF MEMBRANE AIRFOIL COMPARED TO RIGID NACA 4412 AIRFOIL

ABSTRACT

Membrane airfoil is said to have the flexibility to change its surface geometry to adapt to the airflow. This means that it has the potential to balance the pressure gradient, resulting with a delayed stall and also the capability to expand its camber to increase the overall lift. The paper aims to study the aerodynamic performance of a ribbed-structure airfoil (NACA 4412) wrapped in a thin sheet of latex rubber membrane and compare it with the original rigid airfoil. The results from this experiment showed that the lift-to-drag ratio of the membrane airfoil improved when compared to its rigid counterpart with investigations carried out at low Reynolds number from around Re = 30,000 ~100,000. Due to the characteristics of the membrane being frail, high flow velocity will not be suitable. Aerodynamic forces are measured using external force balance at subsonic wind tunnel. Also, this study will attempt to measure the membrane deflections of the airfoil using the concept of elastic modulus.

CIRI-CIRI AERODINAMIK MEMBRAN AIRFOIL DIBANDING DENGAN AIRFOIL ASAL NACA 4412

ABSTRAK

Membran airfoil dikatakan mempunyai fleksibiliti untuk mengubah geometri permukaannya untuk menyesuaikan diri dengan aliran udara. Ini bermakna ia berpotensi untuk mengimbangi tekanan udara yang tidak seimbang, membantu untuk melambatkan proses stalling dan juga keupayaan untuk mengembangkan cambernya untuk meningkatkan lif keseluruhan. Kertas ini bertujuan untuk mengkaji prestasi airfoil (NACA 4412) yang dibalut dengan selapis getah yang nipis dari segi aerodynamik dan membandingkannya dengan airfoil asal yang keras. Hasil daripada eksperimen yang dijalankan pada Reynolds number, Re = 30,000 ~ 100,000 menunjukkan bahawa nisbah lif-to-drag daripada membran airfoil bertambah baik apabila dibandingkan dengan airfoil asal. Disebabkan ciri-ciri membran yang berunsur lemah, aliran udara yang tinggi adalah tidak sesuai. Daya unsur aerodynamik akan diukur menggunakan 'external force balance' dengan terowong anging subsonik. Tambahan pula, kajian ini akan cuba untuk mengukur pengubahan bentuk membran airfoil dengan menggunakan prinsip Young's modulus.

TABLE OF CONTENTS

ENDORSEMENT i
DECLARATION ii
ACKNOWLEDGEMENTS iii
ABSTRACT iv
ABSTRAK v
LIST OF FIGURES vii
LIFT OF TABLES xii
LIST OF ABBREVATIONS xiii
LIST OF SYMBOLS xiv

CHAPTER
1 INTRODUCTION 1
1.1 Research background 1
1.2 Problem statement 5
1.3 Objectives 5
1.4 Scope of work 6
2 LITERATURE REVIEW 7
2.1 Membrane airfoil 7
2.2 Aerodynamics of low Reynolds number 9
3 METHODOLOGY 12
3.1 Experimental apparatus 12
3.1.1 Rubber membrane airfoil 12
3.1.2 Open-circuit wind tunnel (blue colored wind tunnel) 18
3.1.3 Open-circuit wind tunnel with bi-test-section (yellow colored wind tunnel) 19
3.1.4 Three-component-balance 21
3.2 Airfoil testing 26
3.2.1 External balance testing 26
3.2.2 Pressure taps testing 32
4 RESULT AND DISCUSSION 34
4.1 Attachment of latex rubber membrane 34
4.2 Aerodynamic forces 39
4.3 Membrane deformation 46
5 CONCLUSION AND FUTURE WORKS 52

REFERENCES 55
APPENDICES 58
A - Tabulation of lift and drag force readings obtained from the blue wind tunnel 58
B - Tabulation of water manometer readings from the pressure-tapped airfoil from α = -8˚ to 12˚ with interval of 4˚ at speed of around 6.5 m/s 60

LIST OF FIGURES

Figure 1.1: A tiny unmanned aerial vehicle in helicopter form. Figure courtesy of Vision Systems (www.vision-systems.com) 2

Figure 1.2: Prototype of the Harvard Microbiotic Fly, a three-centimeter wingspan flapping-wing robot. Picture taken by Ben Finio, The Harvard Microrobotics Lab. Figure courtesy of PHYSORG (www.phys.org). 3

Figure 1.3: A skeletal wing with 1.01 m wing span wrapped by a 0.5 mm thin membrane. Figure courtesy of Benoît Béguin (Béguin, 2014). 4

Figure 1.4: A semi-membrane wing with rigid leading edge and trailing edge. The wing has a span of 0.564 m and a chord length of 0.22 m. Figure courtesy of Julie Piquee (Piquee and Breitsamter, 2017). 4

Figure 2.1: Airfoil with a solid core being wrapped around by a rubber membrane. Figure courtesy of Rojratsiriku (Rojratsiriku, 2010). 8

Figure 2.2: An example of the membrane upper surface shape obtained from laser sheet visualization. Figure courtesy of Rojratsiriku (Rojratsiriku, 2010). 9

Figure 2.3: Schematic illustration of laminar separation bubble over airfoil upper surface. Figure courtesy of Bob Vanderhoydonck (Vanderhoydonck et al., 2016). 11

Figure 3.1: Model of membrane airfoil 12

Figure 3.2: Setup of test section 1 of the open-circuit wind tunnel with bi-test-section (yellow colored tunnel). Protector is attached outside of the test section. The rigid airfoil is mounted inside the test section. Tufts are attached to the upper surface of the airfoil. Small pressure tubes which connect to the pressure taps are passed through the opening of the mounting shaft to connect with the multi-tube manometer. 13

Figure 3.3: Magnification on top view of the rigid airfoil. The pressure taps of the airfoil are within the drawn red oval shape. 14

Figure 3.4: Dimension of dumbbell specimen cut from Die C standards according to ASTM D412 method 14

Figure 3.5: Tension-strain curve of the rubber latex sheet 15

Figure 3.6: Airfoil structure is being temporary secured to the blue L-beam frame through a bolt and nut. The blue frame is clamped onto the table through 2 G-clamps to stay locked in position. 17

Figure 3.7: The rubber sheet is being firmly gripped by the large bull clip. The clip is hooked onto the spring scale. The top end of the latex rubber sheet was first applied and held (using a finger) onto the trailing edge of the airfoil rib (referring to the airfoil rib located the most-right-end of the wing model). Then, stretching force was applied on the rubber sheet by hand-pulling the spring scale in its longitudinal/axial direction (rubber sheet will be stretched in the chord-wise direction of the wing model). This action will cover the first piece airfoil ribs in its chord-wise direction. 17

Figure 3.8: A portion on the right-end side of the latex rubber sheet has already being attached to the upper camber surface of the airfoil rib. The left-end side of the rubber sheet is being firmly gripped by the large bull clip. The clip was then hooked onto the spring scale. Stretching force is applied on the rubber sheet by hand-pulling the spring scale in its longitudinal/axial direction. The rubber sheet will be stretched in the span-wise direction of the wing model. 18

Figure 3.9: Set-up of open-circuit wind tunnel 19

Figure 3.10: Schematic drawing of the open-circuit wind tunnel. 19

Figure 3.11: Set-up of open-circuit wind tunnel with bi-test-section 20

Figure 3.12: Schematic drawing and general dimensioning (in mm) of the yellow colored wind tunnel 20

Figure 3.13: Three-component-balance (AFA3). Figure courtesy of TecQuipment (www.tecquipment.com) 22

Figure 3.14: General schematic layout of the AFA3 balance. Figure courtesy of TecQuipment (www.tecquipment.com) 22

Figure 3.15: Setup of three-component-balance with the wind tunnel 23

Figure 3.16: A close-up look at the three-component-balance 24

Figure 3.17: Display module of three-component-balance. 24

Figure 3.18: LabVIEW program running on the monitor. 27

Figure 3.19: AFA50 wind tunnel data acquisition system 27

Figure 3.20: Digital differential pressure transducer (AFA5) 28

Figure 3.21: Setup of three-component-balance with mounted membrane airfoil in the test section of the wind tunnel 29

Figure 3.22: Built-in static tube system of the blue wind tunnel consist of a set static pressure tabs surrounding the plenum chamber/settling chamber (right side of figure) and another set that is surrounding the test section (left side of figure). Respective pressure tubes from the settling chamber and from the test section are connected to the pressure transducer to provide pressure-difference readings. 30

Figure 3.23: Set-up of pitot tube and digital manometer at the test section of the blue colored wind tunnel 31

Figure 3.24: Set-up of pressure taps on the rigid airfoil 32

Figure 3.25: Set-up of pitot tube and digital manometer at the test section of the yellow colored wind tunnel 33

Figure 4.1: Isometric view of the airfoil model. From the description in Section 3.1.1 Rubber membrane airfoil, the membrane sheet was attached to the wing model from right to left: panel 1 to panel 4. 35

Figure 4.2: Axis labelling for the rubber sheet and the airfoil model. X-axis moves in the span-wise direction of the wing model, while y-axis moves in chord-wise direction of the model 36

Figure 4.3: Top view of wing-structure model. Number labelling for airfoil ribs. From right side to left side of figure: Airfoil rib No.1, Airfoil rib No.2, Airfoil rib No.3, ... 36

Figure 4.4: Front view of the membrane airfoil model 37

Figure 4.5: Apparatus set-up for attaching rubber sheet to airfoil model 38

Figure 4.6: a) Lift coefficient, b) Drag coefficient, c) Lift-to-drag ratio against angle of attack at 6.5 m/s for membrane airfoil and pressure-tapped airfoil 41

Figure 4.7: a) Lift coefficient, b) Drag coefficient, c) Lift-to-drag ratio against angle of attack for membrane airfoil at different speeds of 5 m/s, 6.5 m/s and 8 m/s 44

Figure 4.8: Membrane airfoil in the test section of blue colored wind tunnel. From top row to bottom row of picture, the wind tunnel was running at an air speed: 5 m/s, 6 m/s and 8.5 m/s. 46

Figure 4.9: a) Geometry of latex rubber membrane airfoil at 6.5 m/s for AOA = 4°, 12°; b) Pressure distribution of latex rubber membrane airfoil at 6.5 m/s for AOA = 4°, 12 47

Figure 4.10: a) Geometry of latex rubber membrane airfoil at 18 m/s for AOA = 4°; b) Pressure distribution of latex rubber membrane airfoil at 18 m/s for AOA = 4°. 48

Figure 4.11: Comparison of membrane airfoil at different freestream velocity. Top of picture: Wind tunnel is running at flow velocity of 4 m/s. Bottom of picture: Wind tunnel is running at flow velocity of 10 m/s. 49

Figure 4.12: U-tube manometers in 3 different configurations. From left to right, the U-tube manometer shows the measurement of static pressure, stagnation pressure and dynamic pressure. Figure courtesy of Bright Hub Engineering (www.brighthubengineering.com). 51

LIFT OF TABLES

Table 3.1: Values of fore, aft and drag tested during the calibration 25

Table 3.2: Values of pressure difference and calculated flow velocity from static pressure tap system and static-pitot tube 31

LIST OF ABBREVATIONS

2D	: Two-dimensional
3D	: Three-dimensional
AOA	: Angle of attack
AR	: Aspect ratio
DLT	: Direct Linear Transformation
LE	: Leading edge
MAV	: Micro air vehicle
TE	: Trailing edge
UAV	: Unmanned aerial vehicle

LIST OF SYMBOLS

ε	: Strain
ΔLe	: Change in length
Le	: Original length
σ	: Stress
F	: Tension
A	: Area of specimen
E	: Modulus of elasticity
L	: Lift
ρ_a	: Air density
v	: Air speed
S	: Wing area
C_l	: Lift coefficient
C_d	: Drag coefficient
L/D	: Lift-to-drag ratio
α	: Angle of attack
Re	: Reynolds number

CHAPTER 1

INTRODUCTION

1.1 Research background

Evolution of airfoil design leads to idea of membrane wings. Membrane wing is a wing that can undergo flexible change in its shape when subjected to aerodynamic loading (Jackson et al., 2001). Compared to a rigid wing, a membrane wing can better adapt to the airflow in attempts to prevent the airfoil from experiencing stall (Shyy et al., 2005). Each flight condition has their own optimal aircraft structure. For instance, the optimal aircraft design for taking-off condition is not necessarily similar to the optimal design for cruise mission (Ninian and Dakka, 2017). That is why having a membrane that could be tailored to various flying conditions is vital to optimize aircraft performance.

Mentioning about membrane airfoils, the topic about micro air vehicle (MAV) must not be left for membrane wings and MAVs are 2 subjects that frequently bump into one another. Micro air vehicle are categorized as a small-scale aircraft with maximum dimension not more than 15 cm and operate under Reynolds number below 10^5 (Hicks, 2009, Rojratsiriku, 2010). Development of micro air vehicle is hugely driven by military purposes to provide surveillance on enemy territory and observation on hazardous environment inaccessible by ground vehicles (Ismail et al., 2014).

As technology advances, memory storage and power sources become smaller and lighter, giving more room for micro air vehicles to improve. Thus, this has generated interest in

researchers to study more on micro air vehicles (Lian et al., 2003, Lian and Shyy, 2005, Ifju et al., 2002). Many micro air vehicle designs, whether it is a fixed wing propeller on a miniature helicopter like in Figure 1.1 or a flapping wing on a robot-fly as in Figure 1.2, they utilize the flexibility of a membrane wing. It is shown that membrane wings can improve longitudinal static stability, delay stall and provide a high lift-to-drag ratio (Rojratsiriku, 2010).

Figure 1.1: A tiny unmanned aerial vehicle in helicopter form. Figure courtesy of Vision Systems (www.vision-systems.com)

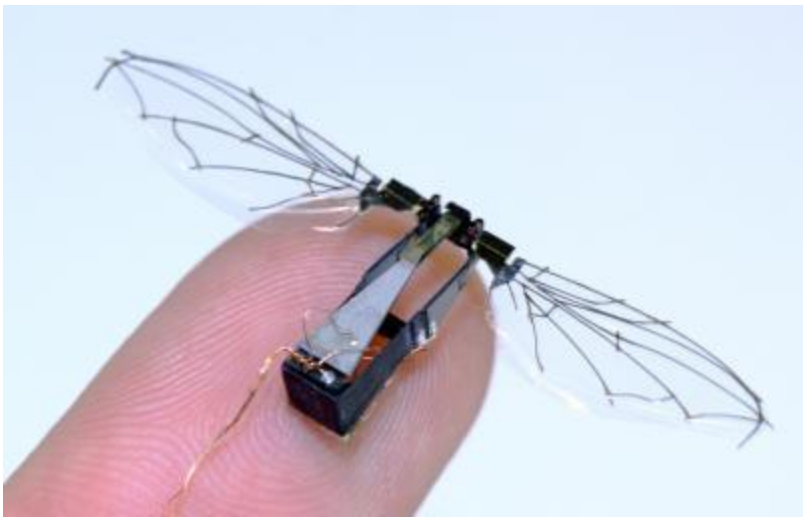

Figure 1.2: Prototype of the Harvard Microbiotic Fly, a three-centimeter wingspan flapping-wing robot. Picture taken by Ben Finio, The Harvard Microrobotics Lab. Figure courtesy of PHYSORG (www.phys.org).

Research is also done on solely membrane wing without specific relation to MAV (Béguin, 2014, Piquee and Breitsamter, 2017). Examples of those wings are illustrated in Figure 1.3 and Figure 1.4. Both works show that flexible wing is capable of mitigating stall. This is because the wing was able to adapt to the adverse pressure, balancing the pressure on the upper side and lower sides of the wing, allowing to flow to stay attached longer. Béguin investigates camber thickness against dynamic pressure (or air speed), where the findings claim that the camber increases in size with increasing air speed. The result is that the lift produced was improved. In the case of Piquee, the camber profile increases with positive angles of attack, resulting in higher lift coefficient.

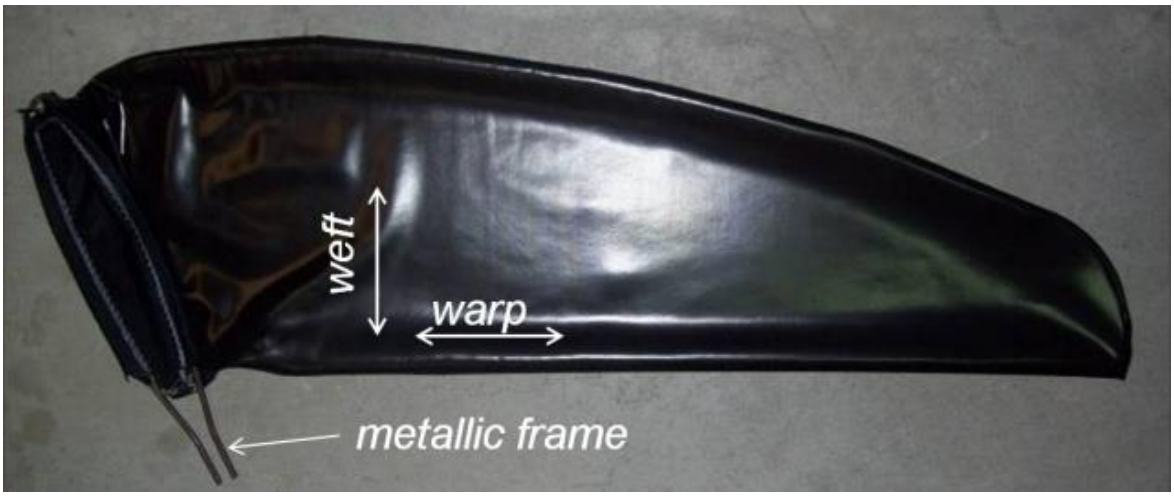

Figure 1.3: A skeletal wing with 1.01 m wing span wrapped by a 0.5 mm thin membrane. Figure courtesy of Benoît Béguin (Béguin, 2014).

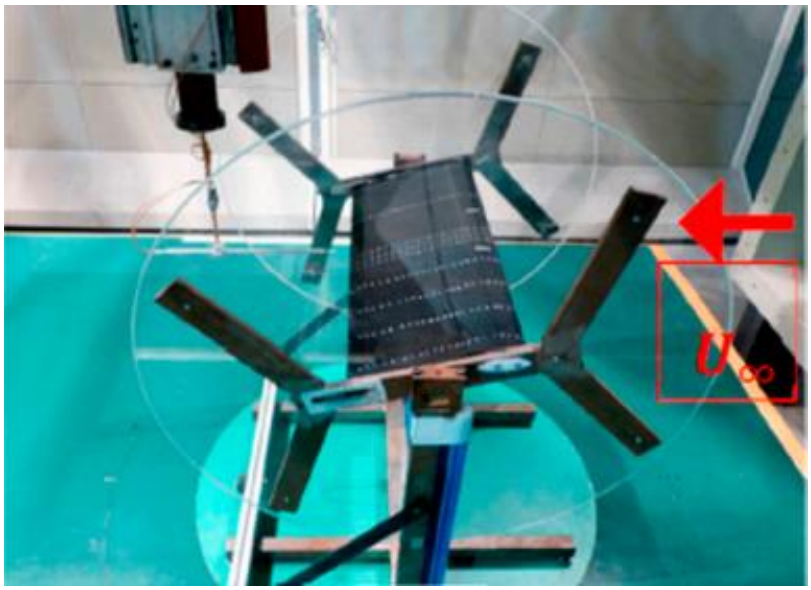

Figure 1.4: A semi-membrane wing with rigid leading edge and trailing edge. The wing has a span of 0.564 m and a chord length of 0.22 m. Figure courtesy of Julie Piquee (Piquee and Breitsamter, 2017).

To understand the fundamental process of those experiments where some important procedures might be unnecessarily left out, this project investigates the aerodynamic capabilities of an in-house-built ribbed wing wrapped by rubber sheet material. Chapter 1 is an introduction on membrane wings where illustrations and definitions are provided to

comprehend the purpose and structure of membrane wings. Chapter 2 reviews previously published literature and research surrounding topic of membrane airfoils and low Reynolds number. The methodology used for current research are presented in Chapter 3, covering the experimental apparatus, data collection procedures and calibration. Chapter 4 outlines the results obtained and discusses the possible causes and solutions to the problems. Chapter 5 summarizes the overall finding of this research and provide suitable recommendations for the future.

1.2 Problem statement

A fully flexible membrane airfoil can morph its shape according to the pressure of the airflow around its body to produce an improved lift-to-drag ratio performance. For a rigid airfoil to be wrapped around by a rubber membrane, its output capability might prove to be similar. It is also important to visualize the deformation of the membrane to understand its behavior when facing various airflow conditions.

1.3 Objectives

This study aims understand if the design of the airfoil model with wings ribs wrapped in a rubber membrane is able to portray as a membrane airfoil that has improved aerodynamic characteristic when compared with the its original rigid NACA 4412 airfoil. It is also important to observe if the proposed method of attaching the membrane to the airfoil is deemed effective in maintaining the shape of the 2D airfoil along the span of its model. The research also attempts to measure the deflection on the membrane of the airfoil through the use of pressure data points from the pressure-taps airfoil.

1.4 Scope of work

An experimental model of membrane airfoil is to be created in-house where it will be tested in the wind tunnel at various angles of attack and at different Reynolds number. Procedures and outcome of attaching the latex rubber membrane onto the airfoil model will be elaborated. Capabilities of the membrane airfoil will be determined by comparing its experimental results with its rigid counterpart.

CHAPTER 2

LITERATURE REVIEW

2.1 Membrane airfoil

Since the Wright brothers, the inspiration for creating wings has always come from flying creatures. Looking especially at gliding mammals, like flying squirrels and bats, they are unique for their flexible membrane wings. These animals showcase remarkable flying performances in terms of their agility and distance with minimal motion (Tamai et al., 2008). If the research on membrane airfoil is able to make a major breakthrough, it could replace the need for control surfaces and high-lift devices on airplane wings, reducing the total weight of the aircraft along with the risk of component failure.

Membrane airfoil is a broad-field term that gets interpreted in different ways by researchers. A membrane airfoil could be a fully flexible gel-like form, a semi-membrane with supporting rigid frames, a rigid structure enclosed in a thin membrane sheet, flapping wings like bats and insects, blades used for turbine (Sugimoto and Kumagai, 1995) and even sails used in sailing boats. The fundamental concept is that the airfoil structure changes its shape according to the incoming airflow.

A particular experimental work of 2-dimensional (2D) airfoil is similar to the research interest of this project. Model of that 2D membrane airfoil is built by (Rojratsiriku, 2010). A 0.2 mm thick latex rubber membrane was wrapped around the solid airfoil structure as in Figure 2.1. Another model was built where tension was being applied to stretch the

membrane prior to attaching it the rigid airfoil core. Method of attaching the rubber membrane was not mentioned. The experimental investigations involves finding the membrane deflection, membrane oscillations, airflow pattern and aerodynamic forces. The end results were subsequently compared with the rigid airfoil.

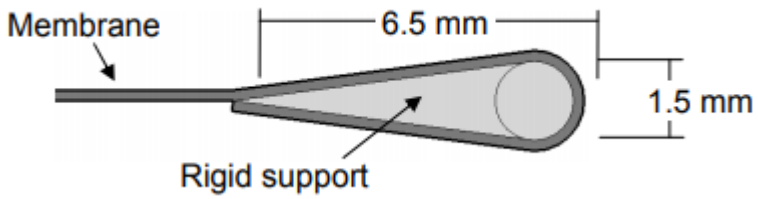

Figure 2.1: Airfoil with a solid core being wrapped around by a rubber membrane. Figure courtesy of Rojratsiriku (Rojratsiriku, 2010).

Membrane deformation can be measured by using a direct visualization method (Rojratsiriku, 2010) or stereophotogrammetry (Piquee and Breitsamter, 2017). The visualization technique places a high speed camera directly in front of the surface of the airfoil chord and the camera is also positioned normal to the flow. An Argon-Ion laser was used to illuminate the membrane surface. The imaged captured will show a white curve as in Figure 2.2. The images were then digitized using the image processing software to determine the coordinates. Due to the multiple images captured for a single take of reading, a time-averaged membrane shape was calculated from the equation,

$$\overline{z} = \frac{1}{N}\sum_{n=1}^{N} z_n \tag{2.1}$$

to obtain the instantaneous coordinate of the membrane. The time-averaged membrane displacement being normal to the chord length is represented by $\overline{z}$. z_n is an instantaneous

membrane displacement and N is the number of image frames produced for that set of reading desired. This visualization technique only detects 2D membrane deflection, which is a disadvantage. The membrane deformation in the span-wise direction could be non-uniform, presenting errors for the membrane displacement in the chord-wise direction.

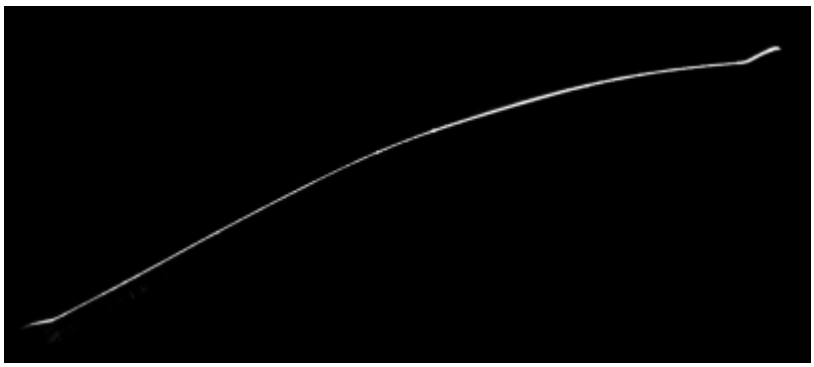

Figure 2.2: An example of the membrane upper surface shape obtained from laser sheet visualization. Figure courtesy of Rojratsiriku (Rojratsiriku, 2010).

The basic idea of stereophotogrammetry is to estimate the 3-dimensional (3D) coordinates of reflective markers marked on the airfoil surface using 2 photographic images taken from 2 cameras. The 2D coordinates captured from the images were converted into 3D coordinates using Direct Linear Transformation (DLT) method (Piquee and Breitsamter, 2017, Béguin, 2014). Béguin states that at least 2 images that shows the projected markers are required to construct the 3D coordinates because one image provides only 2 unknowns, while the DLT equations require 3 unknowns.

2.2 Aerodynamics of low Reynolds number

Low Reynolds number are generally categorized in the range of 10^4 to 10^5 (Tamai et al., 2008). Below than 10, 000 would be termed ultra-low Reynolds number (Kunz, 2003). When speaking of low Reynolds number, it can refer to a fluid that flows very slowly or an

object (in a fluid) that is very small (Purcell, 1977). In the aerodynamics field, both these cases are involved. Suitable examples to represent those interpretation are low freestream velocities at wind tunnels, micro air vehicles (MAV), birds, insects, home-made gliders, radio-controlled unmanned aerial vehicle (UAV).

Low Reynolds number are especially significant and popular in the researches of membrane wings and airfoil (Wrist, 2016, Hu et al., 2008, Hicks, 2009, Aziz, 2012, Gordnier, 2009, Sugimoto and Kumagai, 1995, Tamai et al., 2008). Characteristics of low Reynolds number airfoil are explored to find out its potential and limits. The major issue of concern for airfoil when dealing with low Reynolds number is presence of laminar separation bubble (Essuri et al., 2017, Carmichael et al., 1981). A simple schematic representation of the separation bubble is in Figure 2.3. Laminar separation bubble (LSB) provides the risk of the flow separation at trailing edge, causing airfoil stall, hence poor lift-to-drag ratio. When laminar flow moves downstream of the airfoil upper surface, it eventually faces an adverse pressure gradient at a certain point. If it overcomes the pressure gradient, the flow quickly reattaches and form the separation bubble (Rojratsiriku, 2010).

Laminar separation bubble takes places due to the following sequence of events: a laminar flow separation due to adverse pressure gradient, a turbulent transition within the separated boundary layer, followed by a turbulent reattachment (Crivellini et al., 2014). The presence of laminar separation bubble invites 2 kinds of problem. First, it decreases the lift-to-drag ratio due to the rise in airfoil drag. Large fluctuations occur when the bubble bursts.

The size of the separation bubble is dependent and is in an inverse relationship with Reynolds number. Laminar separation bubble can become bigger and longer as Reynolds number decreases, until the point where it reaches complete separation with no reattachment (Essuri et al., 2017). Investigations done by Shah, 2014 showed that size of the laminar separation bubble reduces with increasing Reynolds number (Shah et al., 2014).

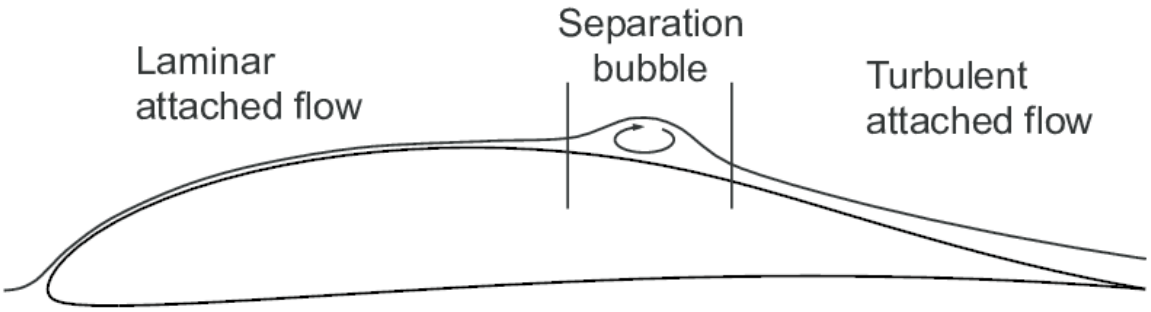

Figure 2.3: Schematic illustration of laminar separation bubble over airfoil upper surface. Figure courtesy of Bob Vanderhoydonck (Vanderhoydonck et al., 2016).

CHAPTER 3

METHODOLOGY

3.1 Experimental apparatus

3.1.1 Rubber membrane airfoil

The airfoil model tested is a 2 dimensional NACA 4412 typed airfoil with a 15 cm chord. It is a ribbed wing wrapped in membrane sheet like in Figure 3.1. For a shorter term, we will name this model as ‘membrane airfoil’. The experiment is complemented with a comparative rigid airfoil with pressure tappings as in Figure 3.2 and Figure 3.3. The membrane airfoil was firstly tested, followed by the rigid airfoil.

Figure 3.1: Model of membrane airfoil

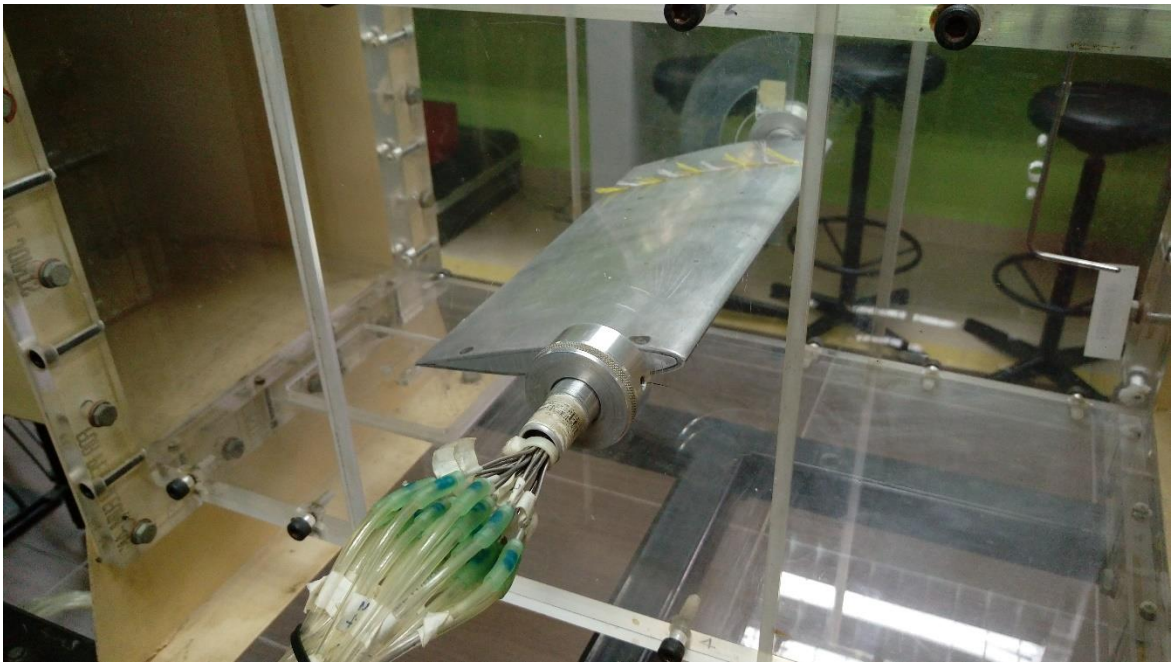

Figure 3.2: Setup of test section 1 of the open-circuit wind tunnel with bi-test-section (yellow colored tunnel). Protector is attached outside of the test section. The rigid airfoil is mounted inside the test section. Tufts are attached to the upper surface of the airfoil. Small pressure tubes which connect to the pressure taps are passed through the opening of the mounting shaft to connect with the multi-tube manometer.

Figure 3.3: Magnification on top view of the rigid airfoil. The pressure taps of the airfoil are within the drawn red oval shape.

The material for the membrane airfoil is made up of a latex rubber sheet, a theraband product from OPPO MEDICAL and distributed by Pinang Medical Supplies. The rubber sheet has a thickness of 0.14 mm and elastic modulus of 2.5 MPa. The elastic modulus of rubber membrane was determined by subjecting it to known tension and extension using the Instron 3366 machine (tensile testing machine) following the ASTM D412 method. The membrane sheet was die-cut into dumbbell specimens of size 115 cm x 25 cm as in Figure 3.4. The gauge length was set at 50 mm and the cross-head speed was controlled at 500 mm/min. The data from the measurements are plotted as in Figure 3.5. The tensile value was calculated by Equations 3.1 to 3.3.

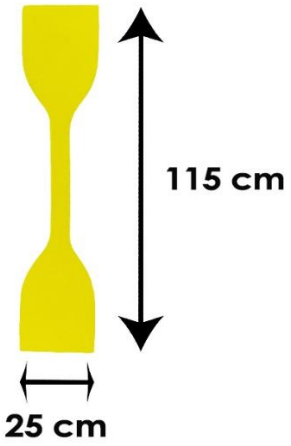

Figure 3.4: Dimension of dumbbell specimen cut from Die C standards according to ASTM D412 method

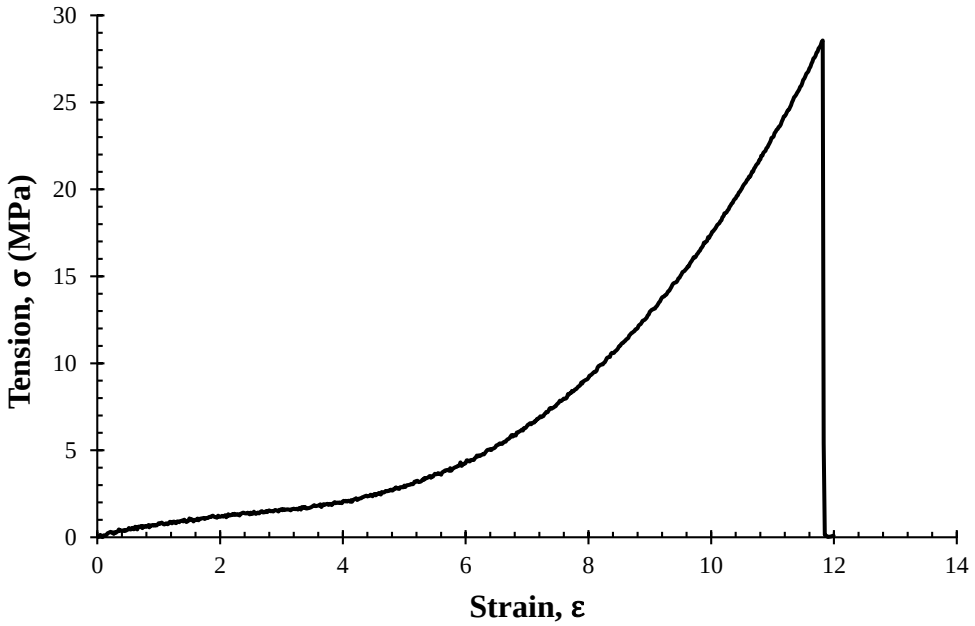

Figure 3.5: Tension-strain curve of the rubber latex sheet

$$\text{Strain}, \varepsilon = \frac{\Delta \text{Le}}{\text{Le}} \tag{3.1}$$

$$\text{Stress}, \sigma = \text{FA} \tag{3.2}$$

$$\text{Elastic modulus}, \text{E} = \frac{\sigma}{\varepsilon} \tag{3.3}$$

The airfoil structure is constructed from 5 perspex ribs. The ribs are separated from one another at a similar distance of 6.125 cm. The gaps allow the deformation of the rubber sheet to occur when subjected to force from the incoming air flow. They are supported by the main mounting shaft made up of mild steel. The shaft is 36 cm long with 6.5 cm of its length being the mounting end. It has an internal thread of 3 cm depth in its mounting end. A 4.1 cm external thread with hexagon nut will be tightly secured between the internal thread and the bore of the three-component-balance (force-measuring instrument), affixing the airfoil model to the measuring equipment. An extra rod, made from balsa wood is installed near

the trailing edge of the model to provide support and prevent independent pitching of the airfoil ribs at their trailing edges.

The rubber sheet was manually wrapped onto the surface of the airfoil ribs with the help of the spring scale and large bull clips. The spring scale is necessary to ensure even amount of force is applied when stretching the rubber membrane along the chord and the span of the airfoil model. With the airfoil structure being locked into place as in Figure 3.6, the rubber membrane is applied onto the airfoil using the method as in Figure 3.7 for chord-wise direction and followed by the method in Figure 3.8 for span-wise direction. The green colored rubber sheet shown in the figures were used as test materials. The final build of the airfoil model is wrapped in yellow rubber membrane. The adhesive used for the attaching the membrane to the airfoil ribs is a thin double-sided tape with 0.08 mm thickness.

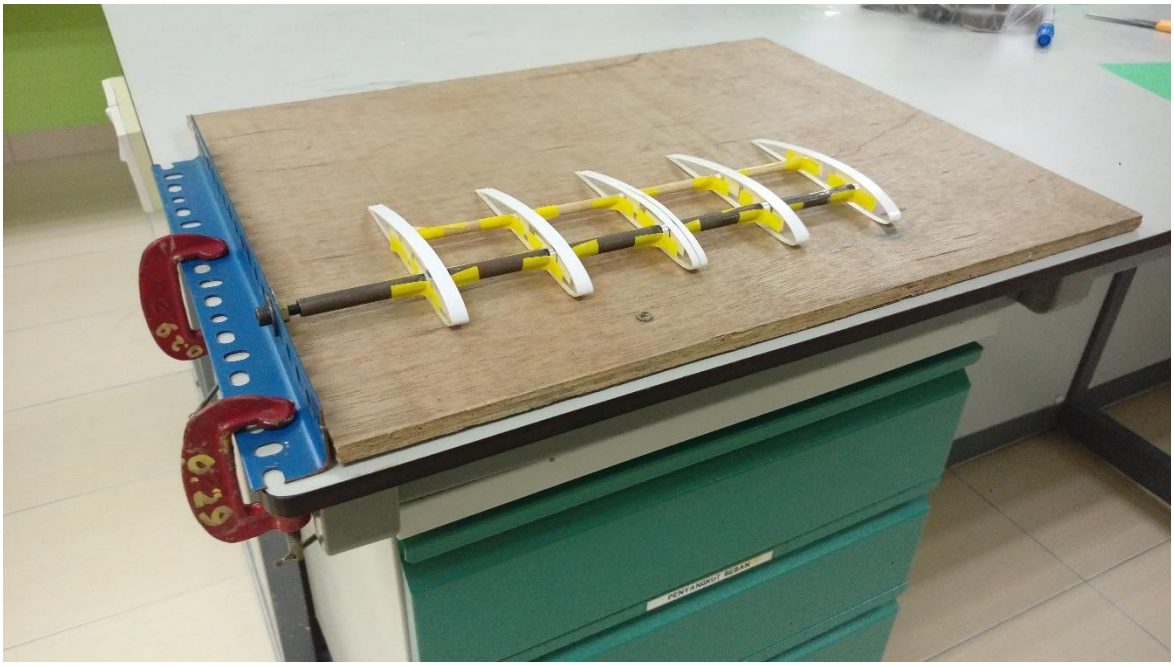

Figure 3.6: Airfoil structure is being temporary secured to the blue L-beam frame through a bolt and nut. The blue frame is clamped onto the table through 2 G-clamps to stay locked in position.

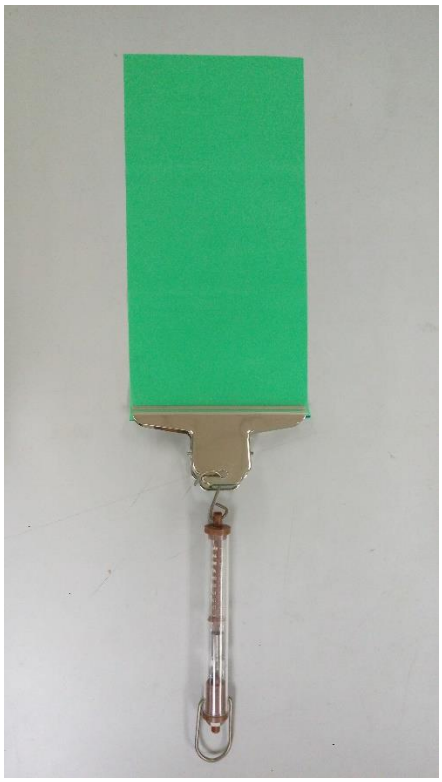

Figure 3.7: The rubber sheet is being firmly gripped by the large bull clip. The clip is hooked onto the spring scale. The top end of the latex rubber sheet was first applied and held (using a finger) onto the trailing edge of the airfoil rib (referring to the airfoil rib located the most-right-end of the wing model). Then, stretching force was applied on the rubber sheet by hand-pulling the spring scale in its longitudinal/axial direction (rubber sheet will be stretched in the chord-wise direction of the wing model). This action will cover the first piece airfoil ribs in its chord-wise direction.

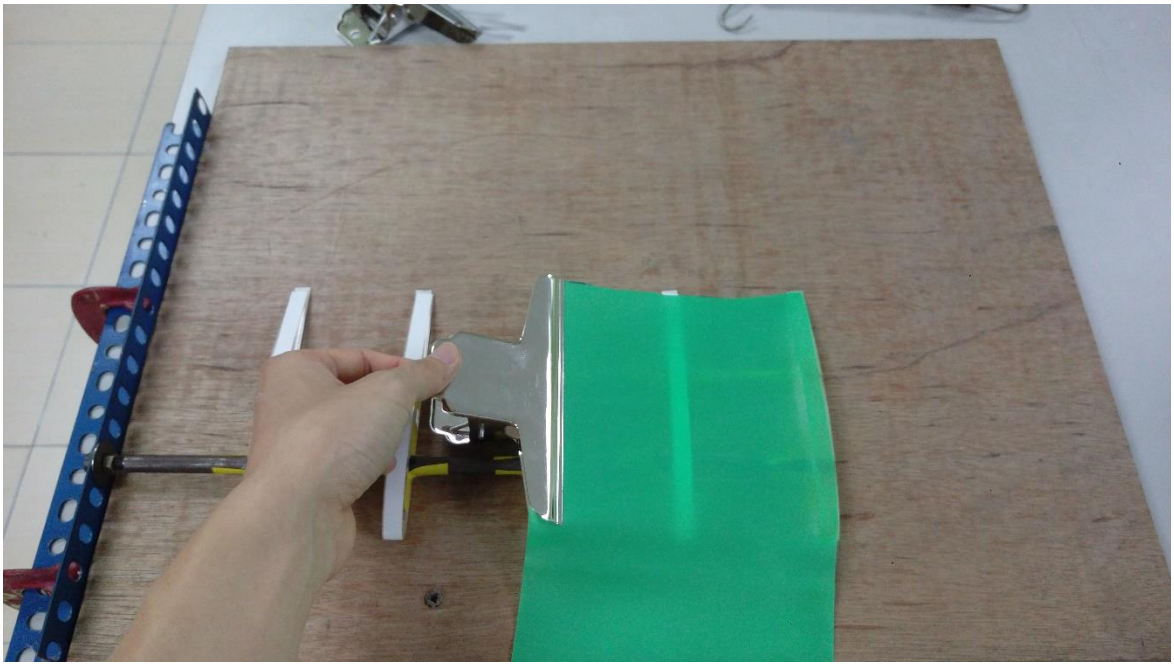

Figure 3.8: A portion on the right-end side of the latex rubber sheet has already being attached to the upper camber surface of the airfoil rib. The left-end side of the rubber sheet is being firmly gripped by the large bull clip. The clip was then hooked onto the spring scale. Stretching force is applied on the rubber sheet by hand-pulling the spring scale in its longitudinal/axial direction. The rubber sheet will be stretched in the span-wise direction of the wing model.

3.1.2 Open-circuit wind tunnel (blue colored wind tunnel)

This subsonic wind tunnel is an open-circuit wind tunnel as in Figure 3.9, a 'ZAF 63.01/C' model from STEM-ISI Impianti. Figure 3.10 shows a schematic drawing of the wind tunnel. The wind tunnel is located in aerodynamics laboratory at the Department of Aerospace Engineering, at the Universiti Sains Malaysia. The structure was bought and installed at 1993. The wind tunnel has a circular working section of 610 millimeters in diameter and 6.32 meters long. The closed test section allows easily accessibility for the placement of models, the use of measuring instrument (pitot-static tube, external force balance) as well as flow visualization through its transparent viewing window. A large fan powered by an

electric motor enables the tunnel to achieve a maximum speed of approximately 36 meters per second.

Figure 3.9: Set-up of open-circuit wind tunnel

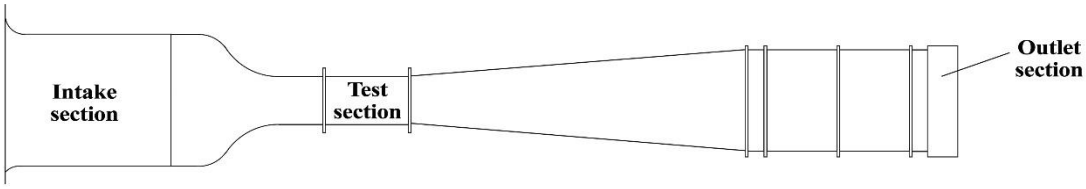

Figure 3.10: Schematic drawing of the open-circuit wind tunnel.

3.1.3 Open-circuit wind tunnel with bi-test-section (yellow colored wind tunnel)

The obvious difference between this wind tunnel and the previous is that this one has an extra test sections in its body. This equipment is that it was not bought in one piece, but an assembly of multiple components: intake section, test section, diffuser, axial fan, settling

chamber. The structure and schematic of the wind tunnel are shown in Figure 3.11 and Figure 3.12.

Figure 3.11: Set-up of open-circuit wind tunnel with bi-test-section

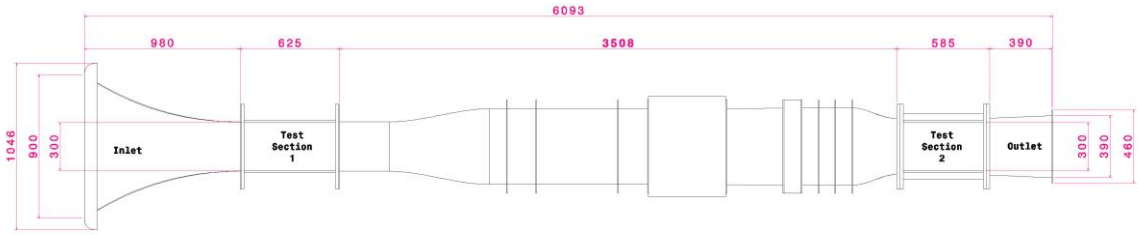

Figure 3.12: Schematic drawing and general dimensioning (in mm) of the yellow colored wind tunnel

Although the wind tunnel has 2 test sections, this project focused on only Test Section 1. Test section 1 is designed to mount the specific 150 mm chord of an airfoil model with pressure tappings. The flexible pressure tubes from the airfoil are connected to the multi-tube manometer for pressure readings. For safety and convenience, the manometer uses

water as the measuring fluid. At the base of the manometer tubes is a reservoir controlled by a shut-off valve at the back of the equipment. The top of each manometer tube is linked to connection piece for tubing to connect to pressure tappings on the airfoil model.

3.1.4 Three-component-balance

The three-component-balance as in Figure 3.13, known as an 'AFA3' unit from TecQuipment. Figure 3.14 shows the schematic construction and main parts of the balance. The main parts of the balance are aluminum alloy. It measures lift, drag and pitching moment exerted on the airfoil model. The AFA3 is a type of external force balance, where it is located external to the airfoil model and the test section of the wind tunnel. In simple terms, the measuring device is placed outside of the test section. The setup can be seen in Figure 3.15.

Figure 3.13: Three-component-balance (AFA3). Figure courtesy of TecQuipment (www.tecquipment.com)

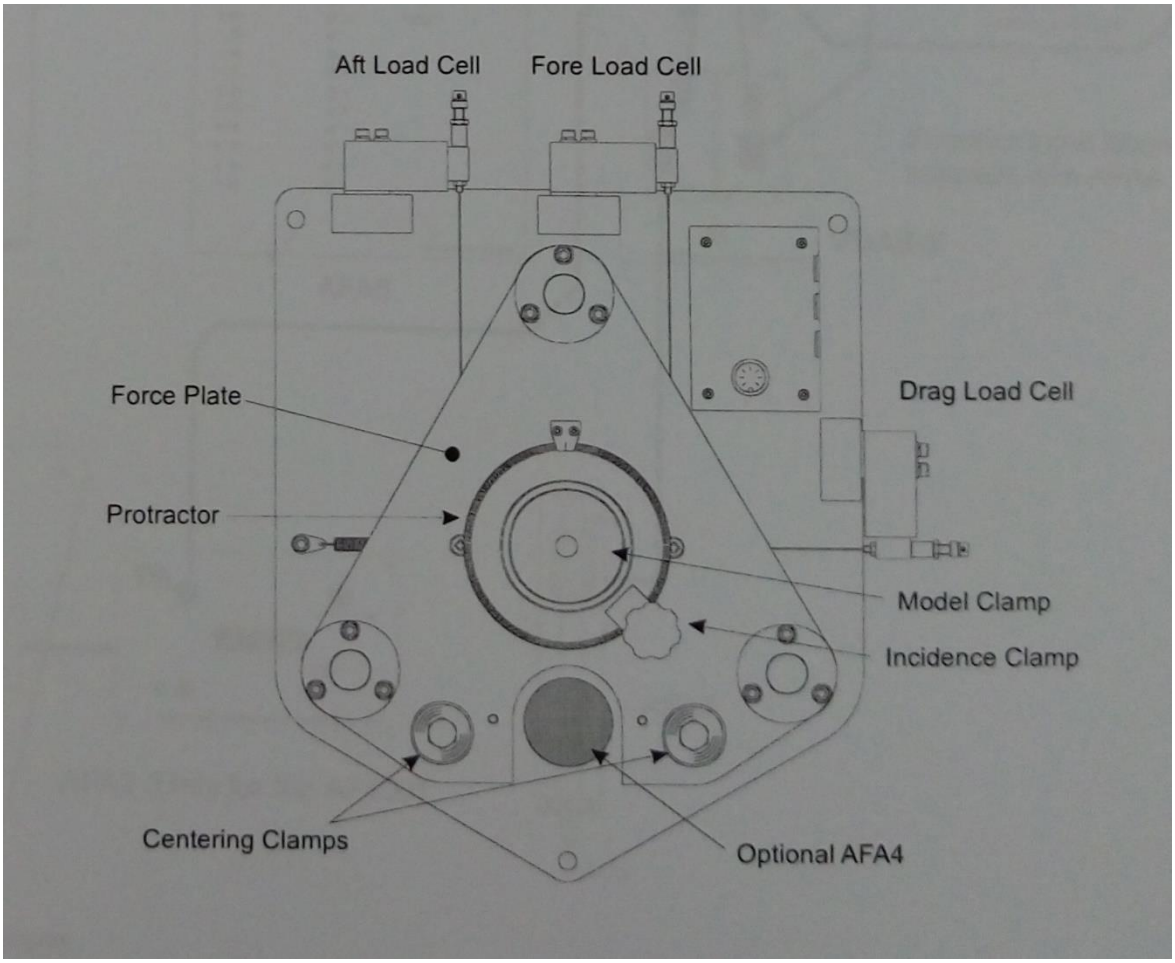

Figure 3.14: General schematic layout of the AFA3 balance. Figure courtesy of TecQuipment (www.tecquipment.com)

Figure 3.15: Setup of three-component-balance with the wind tunnel

The forces acting on the model are transmitted by the tension wires to the load cells. The components can be seen in Figure 3.16. The output from each load cell is taken to a display module. The display module mounts onto the instrumentation frame and includes a digital display to show the lift, drag and pitching moment directly as shown in Figure 3.17.

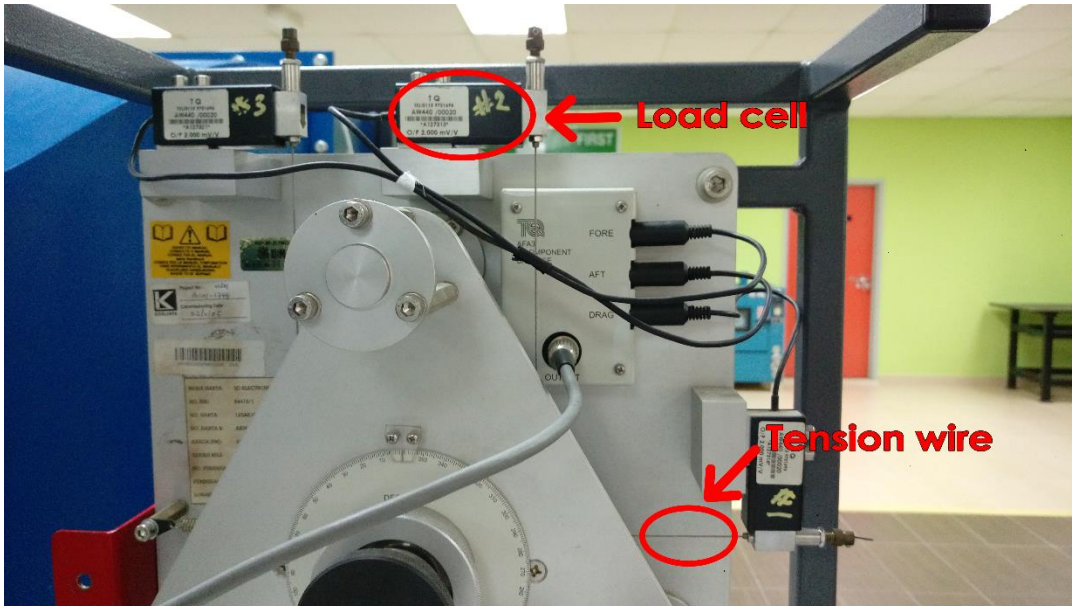

Figure 3.16: A close-up look at the three-component-balance

Figure 3.17: Display module of three-component-balance.